BMC Pulmonary Medicine

RESEARCH

Open Access

PCR array analysis reveals a novel expression profile of ferroptosis-related genes in idiopathic pulmonary fibrosis

Chenyou Shen[1], Wei Wang[1], Dong Wei[1], Xusheng Yang[1], Cheng Jiang[1], Yating Sheng[1], Yuan Chen[1], Jie Sun[2], Xiaoshan Li[3], Guirong Li[1*], Shugao Ye[1*] and Jingyu Chen[1*]

Abstract

Background Idiopathic pulmonary fibrosis (IPF) is a chronic, irreversible, and fatal disease characterized by progressive interstitial lung fibrosis. Given its insidious onset and poor outcome, there is an urgent need to elucidate the molecular mechanisms underlying IPF and identify effective therapeutic targets and diagnosis and prognosis biomarkers. Ferroptosis is an iron-dependent form of programmed cell death that occurs as lipid peroxides accumulate. Growing evidence suggests that ferroptosis is important in IPF.

Methods Human ferroptosis PCR array was performed on IPF and control lung tissue. The differentially expressed ferroptosis-related genes (DE-FRGs) were identified, underwent functional enrichment analyses, protein–protein interaction network construction, and potential drug target prediction. The DE-FRGs were validated and their value as diagnostic and prognostic blood biomarkers were evaluated using the Gene Expression Omnibus dataset GSE28042.

Results The array identified 13 DE-FRGs. Gene Ontology enrichment and Kyoto Encyclopedia of Genes and Genomes pathway analyses revealed that the DE-FRGs were mainly related to iron ion transport, blood microparticles, and oxidoreductase activity, and were involved in porphyrin metabolism, necroptosis, and the p53 signaling pathway in addition to ferroptosis. The 13 DE-FRGs were analyzed using the Drug–Gene Interaction Database to explore novel IPF therapeutic agents, yielding 42 potential drugs. Four DE-FRGs (*BBC3*, *STEAP3*, *EPRS*, *SLC39A8*) in the peripheral blood of IPF patients from the GSE28042 dataset demonstrated the same expression pattern as that observed in the lung tissue array. The receiver operating characteristic analysis demonstrated that the area under the curve of *STEAP3* and *EPRS* were > 0.75. The survival analysis demonstrated that *STEAP3* and *EPRS* were significantly different between the IPF and control groups.

Conclusions The FRG expression profiles in IPF and control lung tissue were characterized. The findings provided valuable ideas to elucidate the role of ferroptosis in IPF and aided the identification of novel IPF therapeutic targets and biomarkers.

Keywords Idiopathic pulmonary fibrosis, Ferroptosis, PCR array, Bioinformatics analysis, Drug targets, Biomarkers

*Correspondence:
Jingyu Chen
chenjy@wuxiph.com
Shugao Ye
ysg206@hotmail.com
Guirong Li
liguirong@njmu.edu.cn
Full list of author information is available at the end of the article

Background

Idiopathic pulmonary fibrosis (IPF) is the most common form of idiopathic interstitial pneumonia and is a chronic, irreversibly progressive, and life-threatening disease with poor clinical outcomes [1, 2]. Epidemiological data demonstrated that the global prevalence of newly diagnosed IPF is 20 cases per 100,000 people per year [3]. IPF is a typical age-related disease that occurs in people aged > 50 years [4], where the estimated survival is 3–5 years if untreated after diagnosis [5]. Nevertheless, the exact cause of IPF remains unknown. Several studies reported the potential risk factors for IPF: genetic variations, lifestyle behaviors, environmental exposures, and viral infections [6]. Although IPF pathogenesis has not been fully elucidated, it is accepted that recurrent injury and aberrant repair of alveolar epithelial cells leads to excessive collagen deposition in the lung, which subsequently develops into pulmonary fibrosis [7].

Given the enigmatic etiology, insidious onset, and dire prognosis of IPF, there is an urgent need for reliable biomarkers enabling early diagnosis and prognosis. Current evidence-based guidelines suggest that the antifibrotic agents pirfenidone and nintedanib are approved for treating IPF. However, in addition to tolerability issues, both drugs exhibit limited efficacy in preventing disease progression and enhancing quality of life [8]. Currently, lung transplantation is the only curative treatment for IPF, which is not an option for most patients due to their age and comorbidities [9]. Given these characteristics, the discovery of effective therapeutic targets for IPF also remains fundamentally important.

Ferroptosis is a unique form of programmed cell death (PCD) that was identified and named a decade ago [10, 11]. Unlike apoptosis, necroptosis, and other forms of PCD, ferroptosis is characterized by the iron-dependent accumulation of hazardous lipid peroxidation products [12]. Ferroptosis has been linked to a wide range of biological properties, including development, immunity, ageing, and cancer [13]. Recently, there has been increasing evidence that ferroptosis is important in lung diseases such as acute lung injury (ALI), chronic obstructive pulmonary disease (COPD), and pulmonary fibrosis [14–16]. Iron accumulation was detected in both in vitro and in vivo models of pulmonary fibrosis and notably in histological samples from IPF patients, revealing some of the underlying mechanisms [17]. For example, TGF-β stimulation upregulated transferrin receptor protein 1 (TFRC) expression in both human and mouse lung fibroblasts, resulting in iron overload, which accelerated fibroblast activation [18]. Additionally, specifically inhibiting UHRF1 arrested ferroptosis formation and impeded pulmonary fibrosis progression in murine models, suggesting UHRF1 as a potential target for treating IPF [19]. However, most studies relating ferroptosis to IPF used cellular and animal models, which are not wholly representative of the process in humans.

Therefore, a systematic understanding of the potential role of ferroptosis in IPF pathogenesis was obtained by collecting lung tissue samples from IPF patients and healthy donors during lung transplantation surgery and conducting PCR arrays of the ferroptosis-related genes (FRGs). Differentially expressed genes (DEGs) specifically associated with ferroptosis were identified and functionally analyzed using bioinformatics. Whether these differentially expressed FRGs (DE-FRGs) can be used as potential diagnostic or prognostic indicators in IPF was investigated by testing the expression of DE-FRGs in peripheral blood mononuclear cells (PBMCs) from IPF patients in the Gene Expression Omnibus (GEO) microarray dataset GSE28042. The genes with similar expression patterns to those detected by our array underwent survival analysis. Overall, the analysis revealed the FRG expression profiles in IPF patients' lung tissue, providing new insights into the underlying mechanism of IPF. We aimed to identify potential diagnosis and prognosis molecular markers and candidate targets for IPF treatment.

Methods

Patients and tissue samples

Fresh lung tissues were obtained from 16 IPF patients who underwent lung transplantation at the Affiliated Wuxi People's Hospital of Nanjing Medical University (Jiangsu, China) between May and December 2019. The control group consisted of lung tissues from 12 healthy donors who were matched to the above recipients during the same period after donor lung volume reduction. We excluded patients with evidence of a known cause of pulmonary fibrosis, such as occupational exposures, autoimmune diseases, medications, and infections. For each case, the lung tissue was divided into two parts: one part was rapidly frozen in liquid nitrogen and stored at -80 °C for preservation, while the other was fixed in 4% paraformaldehyde, then embedded into a paraffin block. Five cases each from the IPF and control groups were randomly selected for PCR array analysis. The remaining cases from both groups were used for expression validation. The Affiliated Wuxi People's Hospital of Nanjing Medical University Institutional Research Ethics Committee approved the human sample collection protocols (2023–126).

RNA extraction and complementary DNA (cDNA) synthesis

The IPF and control lung tissues were transferred from the cryogenic refrigeration system to a liquid nitrogen pre-cooled mortar and ground into powder at low

temperature. Total RNA was extracted using TRIzol (Invitrogen, USA). RNA quality was evaluated via agarose gel electrophoresis. RNA concentration and purity were determined using a NanoDrop 2000 spectrophotometer (Thermo Fisher Scientific, USA). The qualifying RNA samples were reverse-transcribed to cDNA in accordance with the reverse transcription kit instructions (Wcgene Biotech, Shanghai, China). The cDNA and remaining RNA were stored at -80 °C until used.

PCR array

The potential roles of ferroptosis in IPF pathogenesis and progression were explored using a PCR array analysis targeting the ferroptosis-related genes. Gene expression profiles were analyzed using the human ferroptosis PCR array (Wcgene Biotech) according to the manufacturer's protocol. A total of 90 FRGs were examined, including key regulators involved in biological processes such as iron ion metabolism, mitochondrial function regulation, GSH homeostasis maintenance, and redox signaling. Additionally, the PCR array plate included four housekeeping genes for the subsequent internal reference gene selection and target gene expression analysis.

Principal component analysis (PCA)

The array data dimensionality was reduced and the similarities and differences between the control and IPF group samples were evaluated on a global scale using PCA. The analysis was performed in R and visualized using the R ggplot2 package.

Analyses of DEGs

The data were analyzed using Wcgene Biotech software with a screening threshold of |fold change| ≥ 2 and $P < 0.05$ for identifying DEGs. The DEG heat map was generated using the R ComplexHeatmap package. The volcano plot was produced using GraphPad Prism.

Functional enrichment analysis

Gene Ontology (GO) annotation and Kyoto Encyclopedia of Genes and Genomes (KEGG) pathway enrichment analysis of DEGs were conducted using the R clusterProfile package. The GO annotation encompassed biological processes (BP), cellular components (CC), and molecular functions (MF). Reactome enrichment analysis was conducted using the R ReactomePA package. The results were visualized using the R ggplot2 package.

Literature search for DE-FRGs

The molecular mechanisms involved in the effect of DE-FRGs on the pathogenesis of pulmonary fibrosis and their potential role in clinical translational application were explored by systematically searching for each DE-FRG using the PubMed database with the gene name and "pulmonary fibrosis" as keywords.

Correlation heat map

The interrelationships among the DE-FRGs were visualized using a correlation heat map. Spearman correlation analysis was performed in R. The outcomes were visualized using the R ggplot2 package.

Protein–protein interaction (PPI) network construction

The GeneMANIA prediction server (www.genemania.org) integrates biological networks to prioritize genes and gene function prediction [20]. A PPI network of DEGs was constructed using GeneMANIA to evaluate their interactions and functions.

Drug–gene interactions

The Drug–Gene Interaction Database (DGIdb, www.dgidb.org) provides extensive data on drug–gene interactions and druggable genes from credible sources. In this study, potential drugs against the DEGs were predicted using DGIdb to discover new therapeutic targets. The cut-off criterion was a query score > 1 [21]. Subsequently, the drug–gene interaction network was generated using Cytoscape.

Real-time PCR expression validation

The PCR array results were confirmed using real-time PCR, and individual gene expression was examined. Six of the 13 DEGs identified from the array screening were randomly selected and validated in the remaining collected samples (control: 7, IPF: 11). The RNA, which had been previously extracted and stored at -80 °C, was thawed and re-evaluated for concentration and purity. Subsequently, quantitative PCR (qPCR) was performed using the SYBR Green One-Step RT-qPCR Kit (Beyotime, Shanghai, China) on a real-time PCR instrument (Bio-Rad, USA). Table 1 presents the primer sequences. The expression of each gene was normalized to the housekeeping gene *GAPDH*. The relative gene expression was calculated using the comparative threshold cycle ($2^{-\Delta\Delta Ct}$) method.

Immunohistochemical validation of DE-FRGs

Immunohistochemical staining was performed on samples from the validation set (control: 7, IPF: 11) to verify the DEG expression at the protein level. The six genes used for the protein expression verification were the same as those selected for the RNA expression validation described earlier. Wax blocks of lung tissue were cut into 5-μm thick sections, then deparaffinized, rehydrated, and processed for antigen retrieval, blocking, and primary antibody incubation at 4 °C overnight. The primary

Table 1 Real-time PCR primers

Primer	Sequence (5′–3′)
GAPDH	F: TCGGAGTCAACGGATTTGGT
	R: TTCCCGTTCTCAGCCTTGAC
BBC3	F: TGCCTGCCTCACCTTCATC
	R: CTTCAGCCAAAATCTCCCAC
FTMT	F: ATGCGTCCTACGTGTACTTGTC
	R: CCTCCTCGCTGGTTCTGC
STEAP3	F: TGCGTCCACTGCTGTCTTC
	R: ATGTCGTTGAGGCACTTTTGTA
CDO1	F: TTTGATACATGCCATGCCTTTG
	R: GGTGCCCCTTAGTTGTTCTCC
FTH1	F: GGCTGAATGCAATGGAGTGT
	R: TTGATGGCTTTCACCTGCTC
SLC39A8	F: GTTCAGGCTTAGAGGCTTATCG
	R: TGCCATTTGTGAGGGGTG

F Forward, *R* Reverse

antibodies used were: rabbit anti-BBC3 (1:1000; Immunoway, China, YM8416), rabbit anti-FTMT (1:2000; Abcam, USA, ab124889), rabbit anti-STEAP3 (1:1000; Proteintech, USA, 28,478–1-AP), rabbit anti-CDO1 (1:200; Proteintech, 12,589–1-AP), rabbit anti-FTH1 (1:500; CST, USA, 4393S), and rabbit anti-SLC39A8 (1:200; Proteintech, 20,459–1-AP). After incubation with the secondary antibody, DAB chromogenic detection, and hematoxylin counterstaining, the sections were observed and photographed under a light microscope (Olympus, Japan).

GEO database analysis of DE-FRGs in PBMCs

The consistency of DE-FRG expression between lung tissue and blood was investigated by evaluating the DEGs identified in our array by analyzing their expression in PBMCs from IPF patients in a larger population using the GEO GSE28042 dataset. The expression of DE-FRGs identified by our array was assessed using the GSE28042 microarray dataset (platform: GPL6480), which contains the clinical information and gene expression profiles of PBMCs from 19 controls and 75 IPF patients.

Receiver operating characteristic (ROC) and survival analysis

The diagnostic and prognostic potential of DEGs whose expression patterns in GSE28042 PBMCs were concordant with those observed in the lung tissue array were evaluated using ROC and Kaplan–Meier survival analyses. The ROC curve presents the interplay between sensitivity and specificity and is a valuable tool for evaluating diagnostic tests and assessing their predictive accuracy. ROC plots were generated and the relevant parameters (specificity, sensitivity, precision, the Youden index, cutoff value, and the area under the curve [AUC]) were calculated using the R package pROC. The positive and negative likelihood ratios were calculated as follows: positive likelihood ratio = sensitivity/(1—specificity) and negative likelihood ratio = (1—sensitivity)/specificity [22]. Kaplan–Meier analysis was used to compare survival differences between groups. Survival analysis, including the calculation of the number at risk, was performed using Cox regression with the R survival package. The optimal cut-off of the expression value that best separated the survival outcome into two groups was determined for each gene based on the surv-cutpoint function of the R survminer package [23]. The results were visualized using the R survminer and ggplot2 packages.

The analyses evaluating the diagnostic and prognostic potential of the DE-FRGs followed the principles outlined in the STARD 2015 (Standards for Reporting Diagnostic Accuracy Studies) guidelines for reporting diagnostic accuracy [24].

Statistical analysis

Statistical analysis was performed using R 4.2.1 and GraphPad Prism 8.0. All data conformed to the assumption of normal distribution and are presented as the mean ± standard deviation. Comparisons between two groups were made using two-tailed t-tests. A difference of $P < 0.05$ was considered statistically significant.

Results

Baseline characteristics

Figure 1 depicts the flowchart of the overall research design. This study included 16 IPF patients (female: 4, male: 12; mean age: 58.94 ± 8.13 years, age range: 37–74 years) and 12 controls (female: 3, male: 9; mean age: 43 ± 10.85 years, age range: 13–54 years). Pulmonary function [predicted forced vital capacity percentage (FVC%), predicted diffusing capacity of the lung for carbon monoxide percentage (DLCO%), 6-min walk test (6MWT)] was assessed in the IPF patients. Table 2 presents the participants' clinical characteristics.

Identification of DE-FRGs between controls and patients

The specific FRGs that contribute to IPF development were identified by examining the expression patterns of 90 FRGs in the lung tissues of five randomly selected samples each from the control and IPF groups. The PCR array data underwent PCA. The first two principal components (PC) accounted for > 50% of the total data variance, with PC1 explaining 36.4% and PC2 explaining 16.6% of the data variance (Fig. 2A). This demonstrated a distinct distribution of samples between the control and IPF groups.

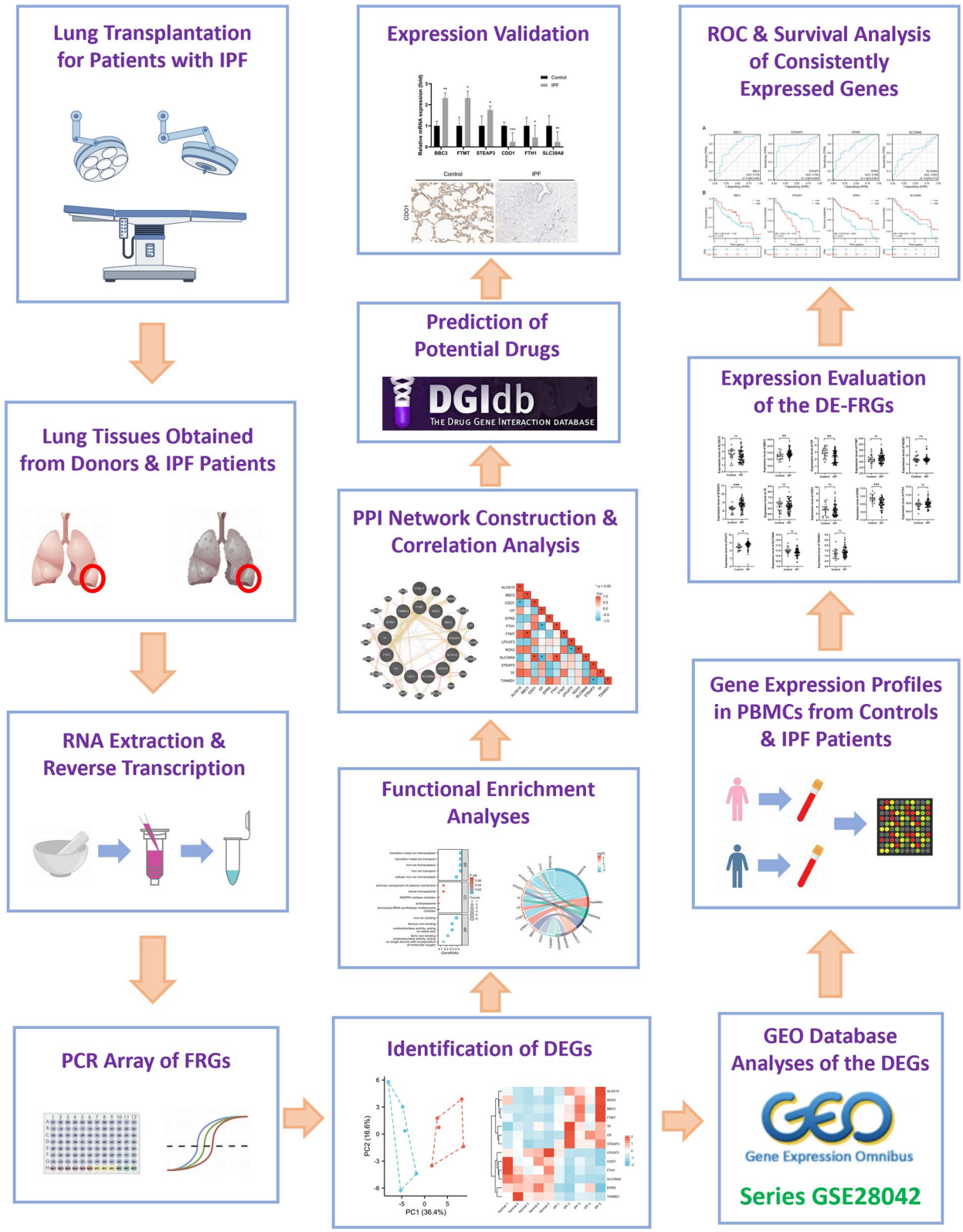

Fig. 1 Flowchart of the overall study design

Table 2 The participants' clinical characteristics

	IPF ($n=16$)	Controls ($n=12$)
Age (years)	58.94 ± 8.13	43 ± 10.85
Sex (female/male)	4/12	3/9
BMI (kg/m^2)	22.82 ± 4.07	26.22 ± 2.92
Former smoker	6 (37.5%)	
Family history	2 (12.5%)	
FVC (%)	41.26 ± 18.02	
DLCO (%)	18.92 ± 11.30	
6MWT (m)	159.5 ± 89.30	

BMI Body mass index, *FVC* Forced vital capacity, *DLCO* Diffusing capacity of the lung for carbon monoxide, *6MWT* 6-min walk test

The screening threshold for the array data was set at |fold change| ≥ 2 and $P < 0.05$. The heatmap illustrates the clustering distribution of samples and DEGs. Of the 90 FRGs examined in the array, the 13 genes marked with a green box showed a distinct expression pattern between the control and IPF groups (Fig. 2B). The volcano plot revealed a consistent pattern with the heatmap, indicating that the IPF group had 13 DE-FRGs compared to the control group. Among the 13 DE-FRGs, seven genes were upregulated (*ALOX15*, *BBC3*, *CP*, *FTMT*, *NOX3*, *STEAP3*, *TF*) and six genes were downregulated (*CDO1*, *EPRS*, *FTH1*, *LPCAT3*, *SLC39A8*, *TXNRD1*) (Fig. 2C). Table 3 presents detailed information regarding the DE-FRGs.

Functional enrichment analyses of DE-FRGs and their potential effect on pulmonary fibrosis

The biological functions of the DE-FRGs and associated signaling pathways were elucidated using GO, KEGG, and Reactome enrichment analyses. A total of 187 GO items, seven KEGG pathways, and 203 Reactome categories were identified and sorted according to the *P*-value. The top five items for each GO category are presented in bubble charts (Fig. 3A), while the seven KEGG pathways are presented using a chord diagram (Fig. 3B). The GO enrichment analysis determined that the DE-FRGs were mainly involved in BP such as iron ion transport, iron ion homeostasis, and transition metal ion transport. The DE-FRGs were primarily related to the CC of blood microparticles, extrinsic component of plasma membrane, and autolysosome. The DE-FRGs were mainly associated with the MF of iron ion binding, ferrous iron binding, and oxidoreductase activity. The KEGG pathway prediction revealed that in addition to ferroptosis, the DE-FRGs were also involved in porphyrin metabolism, mineral absorption, necroptosis, and the p53 signaling pathway. Furthermore, the Reactome analysis indicated that the DE-FRGs were mostly enriched in iron uptake and transport and transport of small molecules (Fig. 3C). Additional file 1: Table S1 details the enriched functional items.

The literature search on the association between DE-FRGs and pulmonary fibrosis identified seven genes with potential influence on pulmonary fibrosis. Some of the genes have potential biomarker roles, such as *CP* and *TF*, others are potential targets for pulmonary fibrosis treatment in in vitro and in vivo models, such as *BBC3* and *EPRS*, and some are downstream targets of certain profibrotic factors or anti-fibrotic agents, such as *NOX3* and *FTH1*. Table 4 details the associations between the DE-FRGs and pulmonary fibrosis.

Correlation analysis and PPI network of DE-FRGs

The relationship between ferroptosis and IPF was examined using expression correlation analysis of the DE-FRGs identified in the array. The correlation heatmap of the 13 DE-FRGs revealed significant negative correlations between *CDO1* and *ALOX15*, *CP* and *FTH1*, *CP* and *SLC39A8*, *NOX3* and *LPCAT3*, and *STEAP3* and *TXNRD1*. There were significant positive correlations between *FTMT* and *BBC3*, *SLC39A8* and *CDO1*, and *SLC39A8* and *FTH1* (Fig. 4A). Furthermore, a PPI network was constructed for the DE-FRGs. The hub nodes represented the 13 DE-FRGs and were surrounded by 20 nodes representing genes that exhibited significant correlations with them (Fig. 4B).

Potential drugs targeting the DE-FRGs

To investigate potential therapeutics for IPF, the 13 DE-FRGs underwent drug prediction analysis using the DGIdb, which identified 42 drugs. Among these drugs, 33 targeted *ALOX15*, while four targeted *CP*, one drug each targeted *TF* and *EPRS1*, and three drugs targeted *TXNRD1*. Figure 5 depicts the drug–gene interaction network. Additional file 2: Table S2 presents detailed information on the sources, query scores, and relevant papers associated with the potential drugs.

RT-qPCR and immunohistochemistry (IHC) validation of the DE-FRGs

The PCR array findings were confirmed using RT-qPCR and IHC. Among the 13 DE-FRGs identified by the array, a six-gene subset (*BBC3*, *FTMT*, *STEAP3*, *CDO1*, *FTH1*, *SLC39A8*) was randomly selected for SYBR Green-based RT-qPCR analysis and immunohistochemical staining. Figure 6A demonstrates that the RT-qPCR expression patterns were consistent with those obtained from the PCR array for all six genes. Consistently, the IHC results demonstrated that BBC3, FTMT, and STEAP3 protein levels were generally positively expressed in the IPF group and weakly or negatively expressed in the control group,

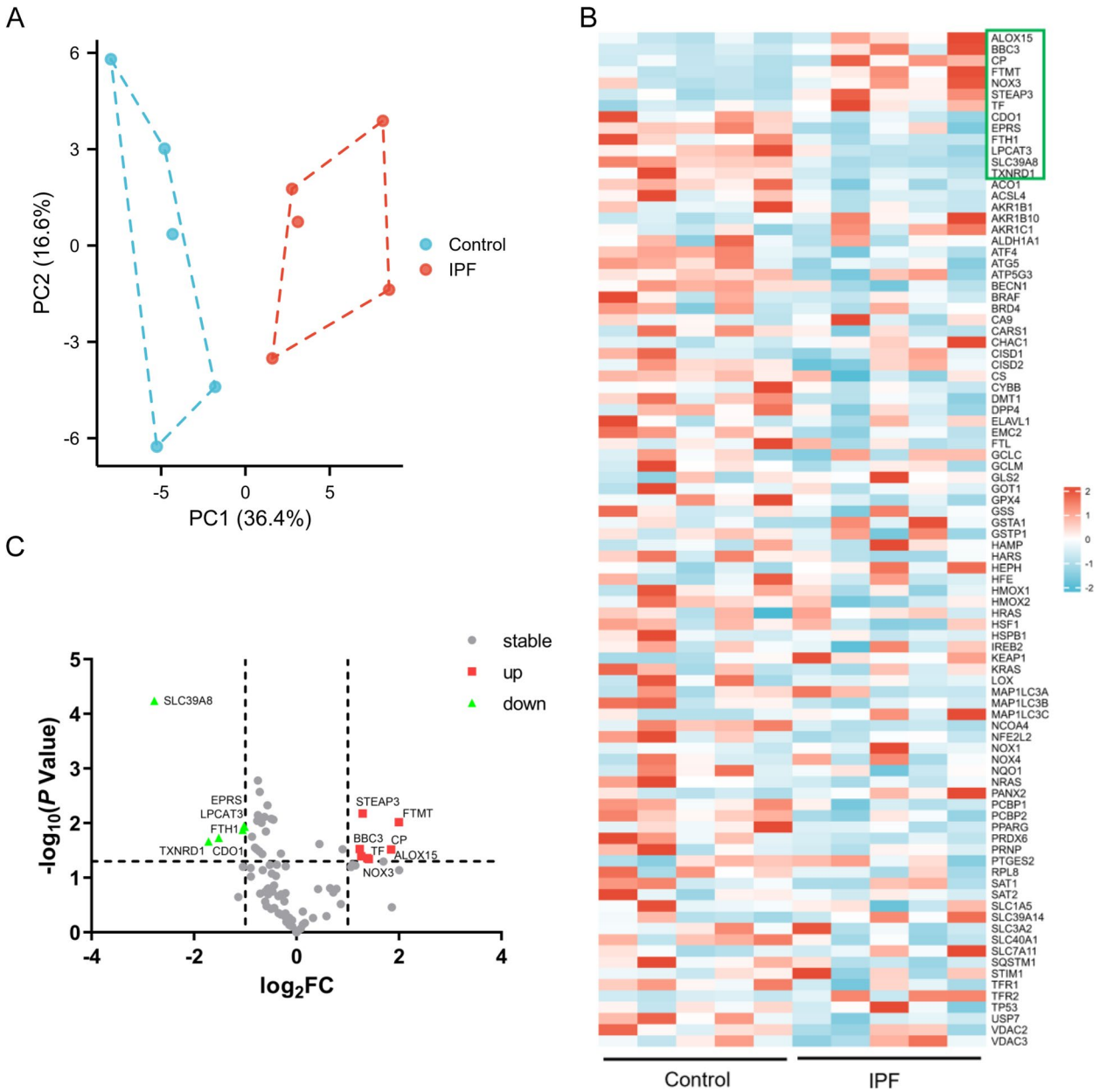

Fig. 2 Identification of DE-FRGs between controls and IPF patients. **A** PCA of control and IPF groups. **B** Heatmap of the FRGs. The green box highlights genes with a significant difference in expression. **C** Volcano plot of the FRG expression profiles

whereas CDO1, FTH1, and SLC39A8 were positively expressed in the control group and weakly expressed in IPF (Fig. 6B).

GEO database analysis of the DE-FRGs

The expression of DE-FRGs in blood was analyzed using the GSE28042 dataset. Consequently, the expression analysis determined that the *BBC3*, *STEAP3*, *EPRS*, and *SLC39A8* expression patterns in the PBMCs were consistent with those observed in our lung tissue array. The opposite was true for the *CP* and *LPCAT3* expression trends, while no significant difference was observed for the remaining genes between the control and IPF groups (Fig. 7).

Identification of diagnostic and prognostic DE-FRGs in the GEO evaluation set

The discriminatory potential of individual genes in differentiating IPF from normal samples was evaluated using ROC analysis of the GSE28042 dataset of the four

Table 3 DE-FRGs between the IPF and control groups

Gene symbol	Description	Fold change	*P*-value
ALOX15	Arachidonate 15-lipoxygenase	↑2.400	0.040
BBC3	BCL2-binding component 3	↑2.349	0.030
CP	Ceruloplasmin	↑3.593	0.030
FTMT	Ferritin mitochondrial	↑3.995	0.010
NOX3	NADPH oxidase 3	↑2.658	0.045
STEAP3	STEAP3 metalloreductase	↑2.448	0.007
TF	Transferrin	↑2.605	0.044
CDO1	Cysteine dioxygenase type 1	↓0.349	0.019
EPRS	Glutamyl-prolyl-tRNA synthetase 1	↓0.492	0.011
FTH1	Ferritin heavy chain 1	↓0.483	0.013
LPCAT3	Lysophosphatidylcholine acyltransferase 3	↓0.496	0.012
SLC39A8	Solute carrier family 39 member 8	↓0.146	0.000
TXNRD1	Thioredoxin reductase 1	↓0.304	0.022

The ↑ and ↓ icons represent upregulated and downregulated genes, respectively

DE-FRGs that exhibited consistent expression patterns in both lung tissue and PBMCs. Figure 8A demonstrates that all four genes had an AUC > 0.6, where the *STEAP3* and *EPRS* AUCs > 0.75. Table 5 lists the other major parameters from the ROC analysis. The prognostic value of the four genes was assessed by survival analysis. The Kaplan–Meier survival curves demonstrated a significantly worse prognosis in patients with high *STEAP3* expression compared to those with low *STEAP3* expression, while patients with high *EPRS* expression exhibited a significantly better outcome compared to those with low *EPRS* expression (Fig. 8B). Additional file 3: Table S3 presents the data grouping for the Kaplan–Meier survival analysis.

Discussion

IPF is a life-threatening lung disease predominantly affecting the elderly population, imposing substantial burdens on both human and material resources, and escalating as a growing socio-economic challenge worldwide. Due to the poor prognosis and lack of effective clinical drug treatments, IPF has been characterized as a cancer-like disorder [32]. Given these circumstances, it is imperative to identify efficacious therapeutic targets and reliable prognostic biomarkers and indicators of drug efficacy for IPF.

Recent evidence suggested that ferroptosis is important in IPF pathogenesis and that inhibiting ferroptosis effectively attenuated pulmonary fibrosis progression in both in vivo and in vitro models [18, 33–35]. Several studies performed bioinformatic analysis by integrating FRGs with DEGs obtained from high-throughput sequencing or microarray data in the GEO database to identify critical FRGs involved in IPF pathogenesis and to elucidate potential prognostic biomarkers [36–38]. In this study, we present for the first time a comprehensive analysis of the FRG expression profiles of IPF patient and healthy donor lung tissue, providing new insights into IPF pathogenesis.

The PCR array used in the present study included 90 key genes involved in the ferroptosis pathway of human cells, covering important BP such as iron ion transport, mitochondrial function regulation, GSH homeostasis maintenance, and redox reaction modulation. Array analysis revealed 13 DEGs in the lung tissue from the IPF patients compared to the controls, where seven genes were upregulated (*ALOX15*, *BBC3*, *CP*, *FTMT*, *NOX3*, *STEAP3*, *TF*) and six genes were downregulated (*CDO1*, *EPRS*, *FTH1*, *LPCAT3*, *SLC39A8*, *TXNRD1*). Most DE-FRGs identified in our array were recently associated with pulmonary fibrosis pathogenesis, where most demonstrated expression patterns consistent with our study. Table 4 details the major effects of the DE-FRGs on pulmonary fibrosis pathogenesis and their potential role in clinical translational applications in IPF.

The DE-FRG functions were explored using GO, KEGG, and Reactome enrichment analyses to yield insights into the underlying mechanisms and prospective clinical translational applications of ferroptosis in IPF. As the array in the present study was based on detecting the expression of 90 ferroptosis-associated genes, ferroptosis was inevitably the most enriched pathway for the DEGs. The clinical translation of ferroptosis in IPF has progressed as research into ferroptosis in IPF has recently intensified. In a recent review, Hu et al. systematically summarized the potential role of therapeutic agents targeting key molecules in ferroptosis in pulmonary fibrosis treatment. A group of compounds

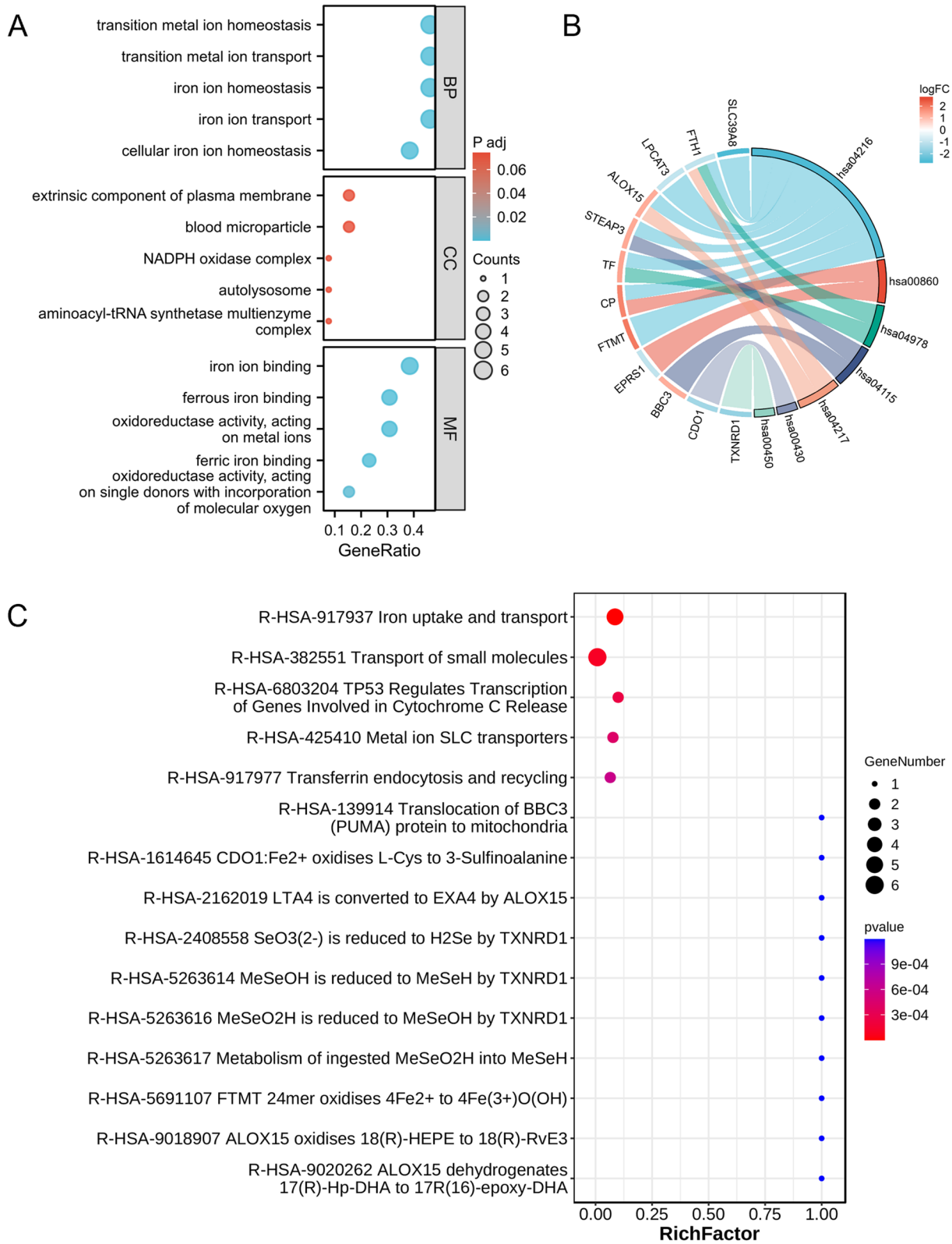

Fig. 3 Functional enrichment analyses of DE-FRGs. **A** Bubble charts of GO enrichment analysis. **B** Chord diagram of KEGG pathway analysis. **C** Bubble chart of Reactome enrichment analysis. Hsa04216, ferroptosis; hsa00860, porphyrin metabolism; hsa04978, mineral absorption; hsa04115, p53 signaling pathway; hsa04217, necroptosis; hsa00430, taurine and hypotaurine metabolism; hsa00450, selenocompound metabolism

Table 4 The influence of identified DE-FRGs on pulmonary fibrosis and their potential role in clinical translational application

Gene	Potential role in the clinical translational application of pulmonary fibrosis	Major effect on pulmonary fibrosis (clinical/preclinical findings)	Ref
BBC3	Potential novel therapeutic target for pulmonary fibrosis	Knockdown of BBC3 expression in vitro and in vivo attenuated silica-induced lung fibrosis by reducing autophagy occurrence	[25]
CP	Potential as a serum biomarker of lung fibrosis	Serum levels of CP were significantly correlated with the exposure levels of respirable fibers in occupational exposure-related pulmonary fibrosis	[26]
NOX3	Downstream target of the profibrotic factor IGFBP-5	IGFBP-5 stimulated transcriptional expression of NOX3 in human fibroblasts. Selective knockdown of NOX3 reduced ROS production by IGFBP-5	[27]
TF	Potential biomarker of IPF	BAL fluid from IPF patients had elevated TF levels compared to controls	[28]
EPRS	Potential therapeutic target for anti-IPF interventions	EPRS regulated the expression of mesenchymal markers and extracellular matrix proteins through TGFβ1–STAT signaling in in vitro and in vivo IPF models	[29]
FTH1	Downstream target of potential pulmonary fibrosis therapeutic DHQ	DHQ suppressed ferritinophagy by upregulating FTH1, attenuating silica-induced pulmonary fibrosis in an in vitro model	[30]
SLC39A8	Potential therapeutic target in pulmonary fibrosis	SLC39A8 deficiency reduced AEC2 regeneration and increased lung fibrosis	[31]

IGFBP-5 Insulin-like growth factor binding protein-5, *ROS* Reactive oxygen species, *BAL* Bronchoalveolar lavage, *DHQ* Dihydroquercetin, *AEC2* Type 2 alveolar epithelial cells

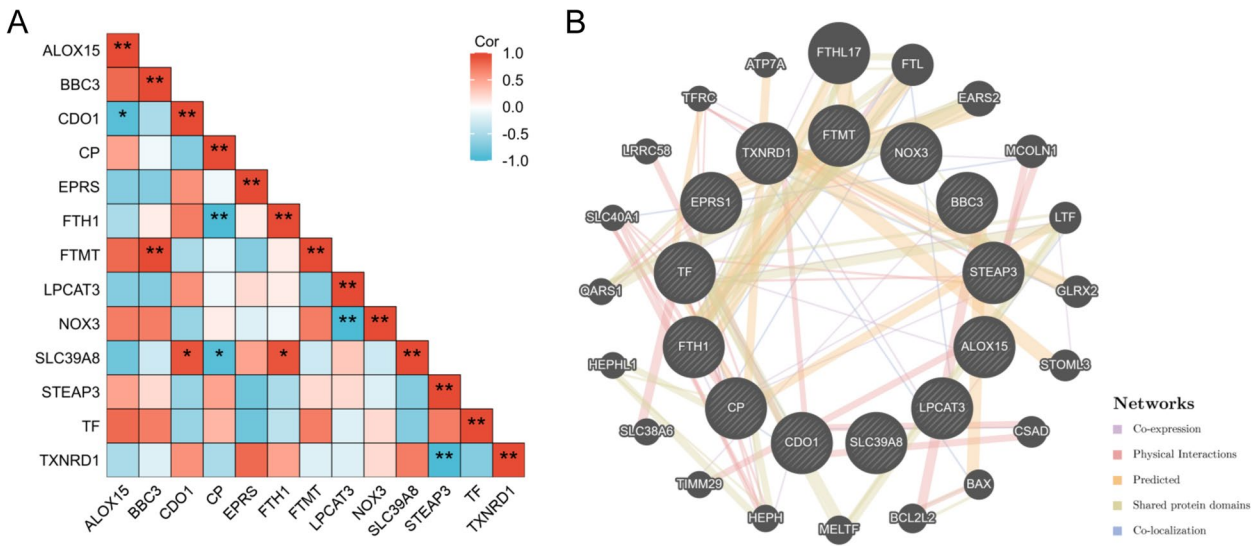

Fig. 4 Correlation and PPI analysis of DE-FRGs. **A** Correlation analysis of DE-FRGs. **B** PPI network of DE-FRGs. **P* < 0.05; ***P* < 0.01

that includes rosiglitazone and empagliflozin offered protection in in vitro and in vivo models of pulmonary fibrosis. These results suggested that these compounds may have clinical translational value in the pharmacological treatment of IPF [39]. Furthermore, Hu et al. provided a comprehensive overview of the potential biomarkers associated with ferroptosis that could be used for the clinical diagnosis and prognosis of pulmonary fibrosis. For example, aconitase 1 in bronchoalveolar lavage fluid and tetrahydrobiopterin in plasma have translational value in assessing the clinical diagnosis and prognosis of IPF [39]. While the porphyrin metabolism pathway has not been directly implicated in IPF, the complex mixture of the porphyrin-containing substance manganese (III) tetrakis (4-benzoate) porphyrin chloride (MnTBAP) attenuated the progression of bleomycin-induced pulmonary fibrosis by acting as a cell-permeable superoxide dismutase (SOD) mimetic and peroxynitrite scavenger [40, 41]. These results suggested a potential therapeutic role for porphyrin metabolism in IPF. The p53 signaling

Fig. 5 The constructed drug–gene interaction network. Orange nodes represent the array-screened DE-FRGs. Green triangles represent the potential drugs identified by the DGIdb database

pathway has been implicated in cellular senescence. Yao et al. reported abnormal p53 activation and regional alveolar type 2 (AT2) cell deficiency in lung tissue from IPF patients. Additionally, the systemic inhibition of p53 in AT2 cells, selective loss of p53 function, or ablation of senescent cells by systemic administration of senolytic drugs attenuated lung fibrosis [42, 43]. Their study suggested that p53-induced AT2 senescence is an important driver and therapeutic target in progressive pulmonary fibrosis. Necrosis was detected in alveolar epithelial type II (AEII) cells from IPF patients associated with *SFTPA1* gene mutations. In vivo studies demonstrated that *Sftpa1* mutation in mice promoted necrosis in AEII cells through JNK-mediated upregulation of *Ripk3*, which exacerbated lung fibrosis, highlighting the necroptosis pathway as a therapeutic target in IPF [44–46]. Regarding the KEGG pathway taurine and hypotaurine metabolism, it was reported decades ago that taurine was protective against pulmonary fibrosis in in vivo models of bleomycin- and radiation-induced pulmonary fibrosis. These studies suggested that taurine metabolism may have a potential translational clinical role in pulmonary fibrosis treatment [47–50]. Significantly for the selenocompound metabolism pathway, Lin et al. recently reported that selenite administration prevented and treated lung function decline and pulmonary fibrosis in mice. Selenite exerted protective effects by inhibiting the proliferation of mouse lung fibroblasts, promoting their apoptosis, and upregulating glutathione reductase and thioredoxin reductase in the mouse lung fibroblasts [51]. That study suggested that selenium metabolism may have important clinical translational value in IPF treatment.

Due to the irreversible nature of IPF and its poor prognosis and the fact that the two currently approved antifibrotic agents for treating IPF (pirfenidone and nintedanib) only impede disease progression but do not cure it, the search for effective drug targets is vital [52, 53]. Therefore, 13 DE-FRGs were analyzed using the DGIdb

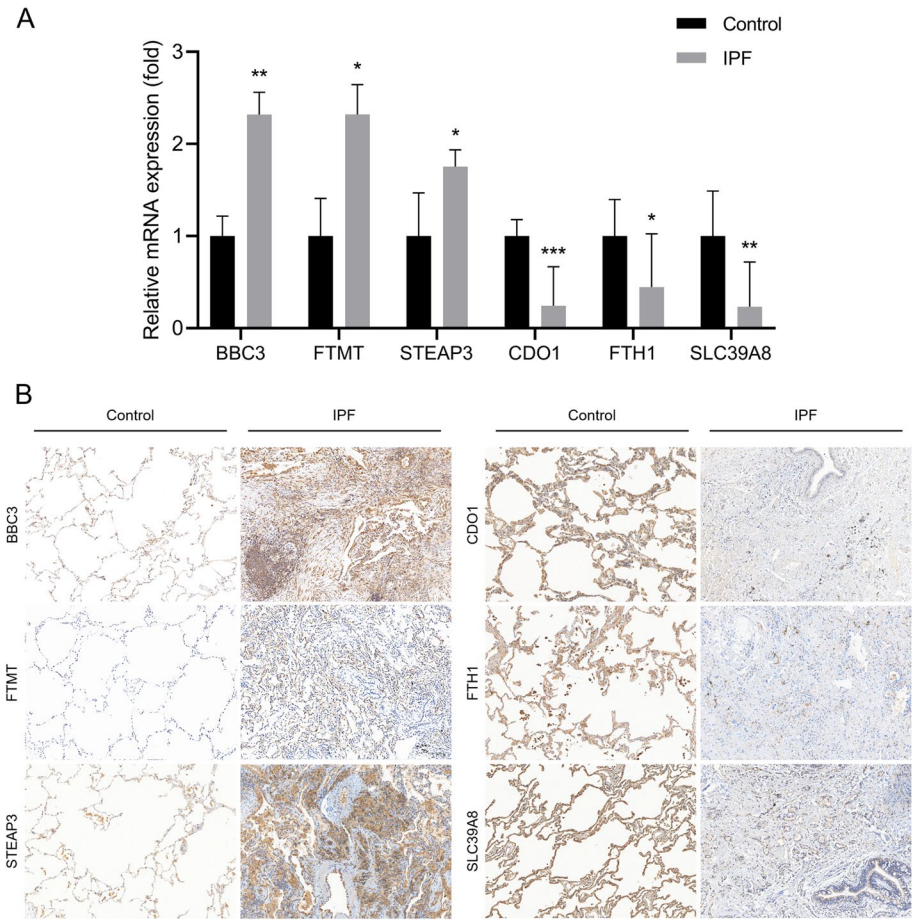

Fig. 6 Expression validation of DE-FRGs. **A** RT-qPCR verified the mRNA expression of six (randomly selected) of 13 DE-FRGs from control ($n=7$) and IPF ($n=11$) lung tissues. *$P<0.05$; **$P<0.01$; ***$P<0.001$. **B** Immunohistochemical analysis revealed the protein expression levels of the six genes in the control ($n=7$) and IPF ($n=11$) lung tissues (×100)

to identify novel therapeutic agents for IPF, and yielded 42 potential drugs. These included synthetic drugs and natural products, some with palliative effects in in vitro or in vivo models of pulmonary fibrosis. Geraniol is a potential drug targeting ALOX15 and is a monoterpene found in the essential oils of fruits, vegetables, and herbs. Geraniol has a wide range of pharmacological activities, including antimicrobial, anti-inflammatory, antioxidant, and anti-cancer [54]. The essential oil of *Cymbopogon winterianus*, of which geraniol is a major component, attenuated bleomycin-induced pulmonary fibrosis in a murine model [55]. Tryptophan is another potential drug targeting ALOX15 and is an amino acid commonly used as a component of total parenteral nutrition. Recent reports suggested that 5-methoxytryptophan, an endogenous molecule derived from tryptophan metabolism, might be a good lead compound for developing novel antifibrotic agents [56]. The soy phytoestrogen isoflavone was predicted to target CP and is a biologically active component found in agriculturally important legumes such as soy and peanut. Incorporating isoflavone in mouse diet attenuated pulmonary fibrosis and improved lung function in mice exposed to hydrochloric acid [57]. Dexrazoxane is another predicted drug against CP and is a cytoprotective drug used to prevent and reduce cardiotoxicity in adults and children with cancer receiving anthracyclines [58, 59]. The potential role of dexrazoxane in protection against bleomycin-induced pulmonary fibrosis in mice has been suggested for decades [60]. The IL-1β inhibitor anakinra is another predicted drug targeting CP. Anakinra reduced TGF-β1 and collagen accumulation in bleomycin-induced mice [61]. Ademetionine, a potential drug targeting TF, is a glutathione precursor and has been used for treating chronic liver disease. Ademetionine effectively reversed the exacerbation of alcohol-induced lung fibrosis in a mouse model of bleomycin-induced lung fibrosis [62]. Halofuginone is a potential drug targeting EPRS1 and is a low-molecular weight quinazolinone alkaloid that potently inhibits collagen type I gene expression. The role of halofuginone in

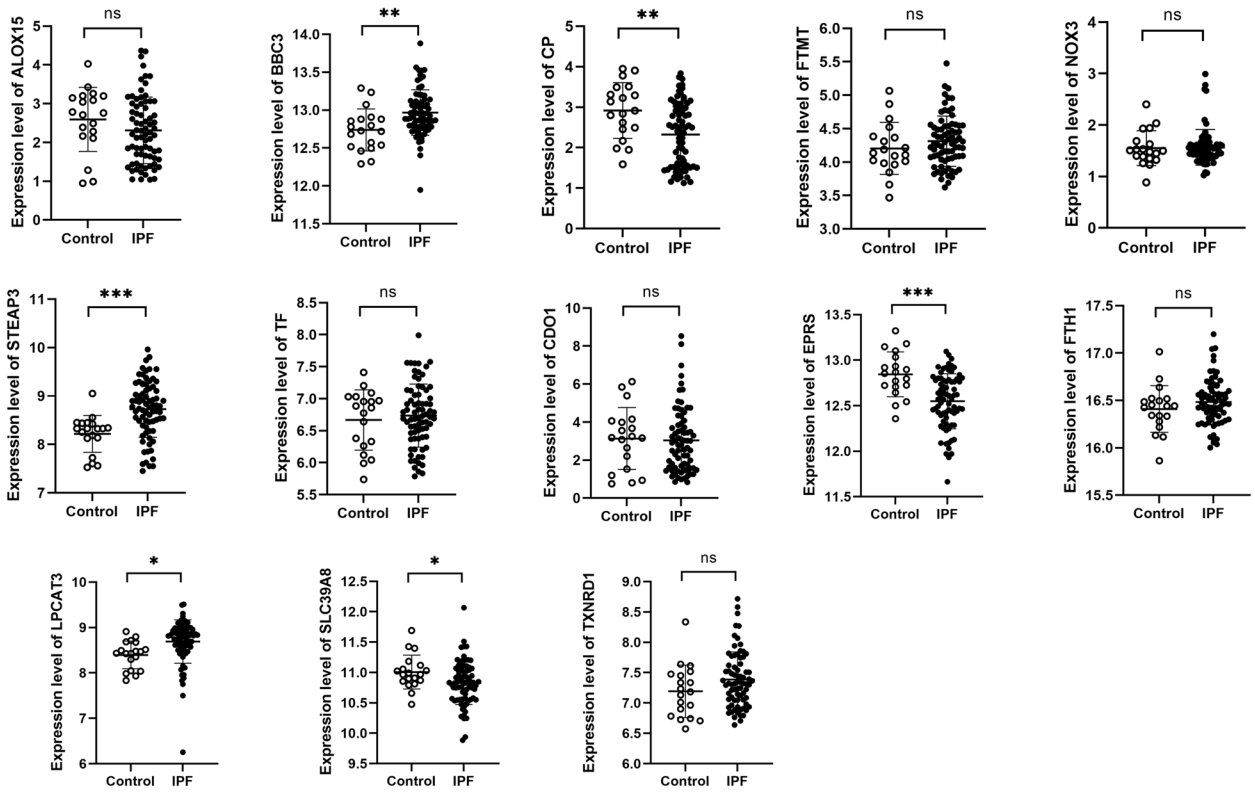

Fig. 7 GEO database expression analysis of DE-FRGs. The mRNA expression levels of DE-FRGs in PBMCs from controls ($n = 19$) and IPF patients ($n = 75$) of the GSE28042 dataset are shown. *$P < 0.05$; **$P < 0.01$; ***$P < 0.001$; ns, no significance

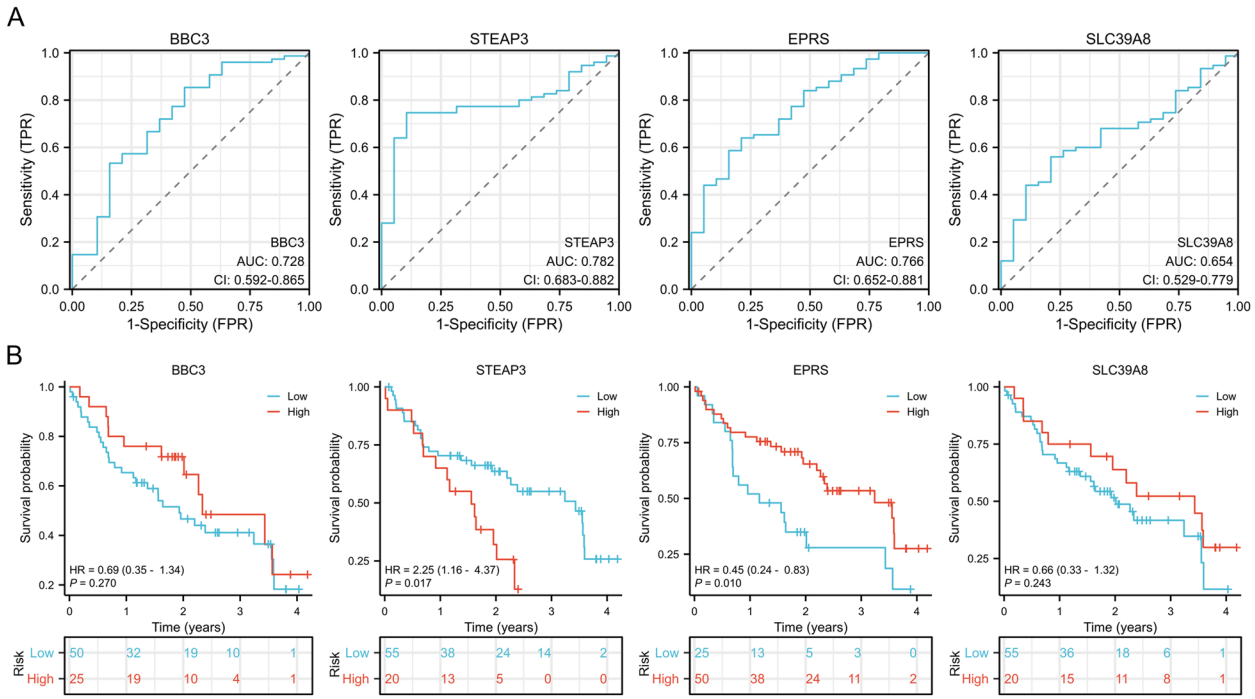

Fig. 8 Diagnostic and prognostic performance of the DE-FRGs using the GEO database. ROC analysis (**A**) and Kaplan–Meier survival curves (**B**) of the four DE-FRGs that demonstrated consistent expression patterns between lung tissue identified by our array and GSE28042 PBMCs are shown

Table 5 Relevant parameters of the ROC analysis

Variant	Specificity	Sensitivity	Precision	Youden index	Cut-off value	LR +	LR-
BBC3	0.53	0.85	0.79	0.38	12.73	1.80	0.28
STEAP3	0.89	0.75	0.78	0.64	8.46	7.09	0.28
EPRS	0.79	0.64	0.67	0.43	12.70	3.04	0.46
SLC39A8	0.79	0.56	0.61	0.35	10.85	2.66	0.56

LR + Positive likelihood ratio, *LR*- Negative likelihood ratio

preventing bleomycin-induced pulmonary fibrosis formation in vivo was indicated decades ago [63]. Spermidine is a predicted drug of TXNRD1 and is a polyamine formed from putrescine and spermine precursor. Spermidine attenuated bleomycin-induced lung fibrosis in mice by inducing autophagy and inhibiting ERS-induced cell death [64]. Arsenic trioxide is another predicted drug against TXNRD1 and is a naturally toxic substance that causes various dangerous side effects. Despite being a poison, arsenic trioxide is important as a chemotherapeutic agent for treating leukemia that does not respond to first-line agents [65, 66]. Furthermore, arsenic trioxide inhibited both the functions of TGF-β1-induced lung fibroblasts in vitro and bleomycin-induced lung fibrosis in vivo [67, 68].

While blood biomarkers aid the assessment of diagnosis, prognosis, and treatment response, none are currently integrated into clinical decision-making [69–72]. Accordingly, the expression of DE-FRGs in peripheral blood was validated and their value in IPF diagnosis and prognosis was validated via array-derived DE-FRGs in the GSE28042 dataset. Four genes with consistent expression trends between the arrayed lung tissue and the GEO PBMCs were identified: *BBC3*, *STEAP3*, *EPRS*, and *SLC39A8*. ROC analysis demonstrated that *BBC3*, *STEAP3*, and *EPRS* had AUCs > 0.7, suggesting a diagnostic reference value. Furthermore, survival analysis revealed that patients with high blood STEAP3 expression had a worse prognosis, which was consistent with the upregulation of STEAP3 in the individuals with IPF. In contrast, patients with high blood EPRS expression had a more favorable prognosis, which was also consistent with the downregulation of EPRS in the IPF patients.

Taken together, ferroptosis is important in IPF pathogenesis, although the underlying mechanism remains to be elucidated. Our study relied primarily on fresh, native samples obtained from transplant patients and therefore provides a valuable resource for studying the role of ferroptosis in IPF. However, our study has some limitations. First, the lack of patients' blood samples in this study precluded the evaluation of potential biomarker expression in blood, thereby reducing the clinical translational value of the study. Second, due to the effect of the coronavirus disease 2019 (COVID-19) pandemic and time constraints, we included a small number of patient samples, which reduced statistical power. Furthermore, the donor samples were mostly from brain-dead patients with accidental injuries and who were generally younger, whereas the IPF samples were mostly from elderly patients, which prevented a good age match between the control and IPF groups. The next phase of our work will involve refining the data by increasing patient sample size and validating the expression of potential biomarkers in blood samples. Lastly, the efficacy of the drug candidates and specific mechanisms by which the DEGs regulate IPF progression through ferroptosis will be investigated via in vitro and in vivo experiments.

Conclusion

We characterized the FRG expression profiles in IPF and control lung tissues via PCR array analysis. We then identified the DEGs and performed functional analyses to elucidate their roles. Furthermore, we predicted potential drug targets based on these findings and integrated GEO data to identify promising blood biomarkers for IPF diagnosis and prognosis. Further experimental studies are needed to confirm our findings and to clarify the role of DE-FRGs in IPF pathogenesis.

Abbreviations

IPF	Idiopathic pulmonary fibrosis
PCD	Programmed cell death
ALI	Acute lung injury
COPD	Chronic obstructive pulmonary disease
DEGs	Differentially expressed genes
FRGs	Ferroptosis-related genes
DE-FRGs	Differentially expressed ferroptosis-related genes
PBMCs	Peripheral blood mononuclear cells
GEO	Gene Expression Omnibus
PCA	Principal component analysis
GO	Gene Ontology
KEGG	Kyoto Encyclopedia of Genes and Genomes
BP	Biological processes
CC	Cellular components
MF	Molecular functions
PPI	Protein–protein interaction
DGIdb	Drug–Gene Interaction Database
ROC	Receiver operating characteristic
AUC	Area under the curve
FVC	Forced vital capacity
DLCO	Diffusing capacity of the lung for carbon monoxide
6MWT	6-Minute walk test

ERS	Endoplasmic reticulum stress
IHC	Immunohistochemistry
HRCT	High-resolution computed tomography
ROS	Reactive oxygen species
BAL	Bronchoalveolar lavage
ECM	Extracellular matrix
AEC2	Type 2 alveolar epithelial cells
COVID-19	Coronavirus disease 2019

Supplementary Information

The online version contains supplementary material available at https://doi.org/10.1186/s12890-025-03555-7.

Additional file 1. Table S1. GO, KEGG, and Reactome enrichment analyses of the DE-FRGs.

Additional file 2. Table S2. Drugs predicted to interact with the DE-FRGs according to the DGIdb database.

Additional file 3. Table S3. Data grouping for the Kaplan-Meier survival analysis.

Acknowledgements
Not applicable.

Authors' contributions
CS conceived the study, analyzed the data, and drafted the manuscript. WW, DW, XY, and CJ performed the experiments and interpreted the results. YS and YC collected the clinical samples. JS and XL collected the clinical information. GL conducted the statistical analysis. SY and JC directed and acquired financial support for the study. All authors read and approved the final manuscript.

Funding
This study was supported by the National Natural Science Foundation of China (No. 82070059), the Lung Transplant Medical Innovation Center Project of Jiangsu (No. CXZX2022001), and the Medical Project of Wuxi Science and Technology Department (No. Y20222007).

Data availability
The data generated and analyzed from our center are included in this article, along with the supplementary information files. A public dataset was downloaded and analyzed in this study, which can be found in the GEO repository under accession number GSE28042.

Declarations

Ethics approval and consent to participate
The Affiliated Wuxi People's Hospital of Nanjing Medical University Institutional Research Ethics Committee approved the human sample collection protocols (2023–126). The donors and recipients enrolled in the study or their family members signed informed consent forms.

Consent for publication
Not applicable.

Competing interests
The authors declare no competing interests.

Author details
[1]Lung Transplant Center, The Affiliated Wuxi People's Hospital of Nanjing Medical University, Wuxi People's Hospital, Wuxi Medical Center, Nanjing Medical University, 299 Qingyang Road, Wuxi 214023, Jiangsu, China. [2]Department of Scientific Research, The Affiliated Wuxi People's Hospital of Nanjing Medical, University, Wuxi People's Hospital, Wuxi Medical Center, Nanjing Medical University, 299 Qingyang Road, Wuxi 214023, Jiangsu, China. [3]Organ Donation and Transplant Management Office, The Affiliated Wuxi People's Hospital of Nanjing Medical University, Wuxi People's Hospital, Wuxi Medical Center, Nanjing Medical University, 299 Qingyang Road, WuxiJiangsu 214023, China.

Received: 8 February 2024 Accepted: 12 February 2025
Published online: 28 February 2025

References

1. Lederer DJ, Martinez FJ. Idiopathic pulmonary fibrosis. N Engl J Med. 2018;378:1811–23.
2. Richeldi L, Collard HR, Jones MG. Idiopathic pulmonary fibrosis. Lancet. 2017;389:1941–52.
3. Rubio K, Singh I, Dobersch S, Sarvari P, Gunther S, Cordero J, et al. Inactivation of nuclear histone deacetylases by EP300 disrupts the MiCEE complex in idiopathic pulmonary fibrosis. Nat Commun. 2019;10:2229.
4. Diamantopoulos A, Wright E, Vlahopoulou K, Cornic L, Schoof N, Maher TM. The burden of illness of idiopathic pulmonary Fibrosis: a comprehensive evidence review. Pharmacoeconomics. 2018;36:779–807.
5. Chung KP, Hsu CL, Fan LC, Huang Z, Bhatia D, Chen YJ, et al. Mitofusins regulate lipid metabolism to mediate the development of lung fibrosis. Nat Commun. 2019;10:3390.
6. Phan THG, Paliogiannis P, Nasrallah GK, Giordo R, Eid AH, Fois AG, Zinellu A, Mangoni AA, Pintus G. Emerging cellular and molecular determinants of idiopathic pulmonary fibrosis. Cell Mol Life Sci. 2021;78:2031–57.
7. Spagnolo P, Kropski JA, Jones MG, Lee JS, Rossi G, Karampitsakos T, Maher TM, Tzouvelekis A, Ryerson CJ. Idiopathic pulmonary fibrosis: Disease mechanisms and drug development. Pharmacol Ther. 2021;222:107798.
8. Li R, Jia Y, Kong X, Nie Y, Deng Y, Liu Y. Novel drug delivery systems and disease models for pulmonary fibrosis. J Control Release. 2022;348:95–114.
9. George PM, Patterson CM, Reed AK, Thillai M. Lung transplantation for idiopathic pulmonary fibrosis. Lancet Respir Med. 2019;7:271–82.
10. Dixon SJ, Lemberg KM, Lamprecht MR, Skouta R, Zaitsev EM, Gleason CE, et al. Ferroptosis: an iron-dependent form of nonapoptotic cell death. Cell. 2012;149:1060–72.
11. Angeli JPF, Shah R, Pratt DA, Conrad M. Ferroptosis Inhibition: Mechanisms and opportunities. Trends Pharmacol Sci. 2017;38:489–98.
12. Djulbegovic MB, Uversky VN. Ferroptosis - An iron- and disorder-dependent programmed cell death. Int J Biol Macromol. 2019;135:1052–69.
13. Stockwell BR. Ferroptosis turns 10: Emerging mechanisms, physiological functions, and therapeutic applications. Cell. 2022;185:2401–21.
14. Ma A, Feng Z, Li Y, Wu Q, Xiong H, Dong M, Cheng J, Wang Z, Yang J, Kang Y. Ferroptosis-related signature and immune infiltration characterization in acute lung injury/acute respiratory distress syndrome. Respir Res. 2023;24:154.
15. Xia H, Wu Y, Zhao J, Cheng C, Lin J, Yang Y, Lu L, Xiang Q, Bian T, Liu Q. N6-Methyladenosine-modified circSAV1 triggers ferroptosis in COPD through recruiting YTHDF1 to facilitate the translation of IREB2. Cell Death Differ. 2023;30:1293–304.
16. Yue D, Zhang Q, Zhang J, Liu W, Chen L, Wang M, Li R, Qin S, Song X, Ji Y. Diesel exhaust PM2.5 greatly deteriorates fibrosis process in pre-existing pulmonary fibrosis via ferroptosis. Environ Int. 2023; 171:107706.
17. Ali MK, Kim RY, Brown AC, Donovan C, Vanka KS, Mayall JR, et al. Critical role for iron accumulation in the pathogenesis of fibrotic lung disease. J Pathol. 2020;251:49–62.
18. Pei Z, Qin Y, Fu X, Yang F, Huo F, Liang X, et al. Inhibition of ferroptosis and iron accumulation alleviates pulmonary fibrosis in a bleomycin model. Redox Biol. 2022;57:102509.
19. Liu Y, Cheng D, Wang Y, Xi S, Wang T, Sun W, Li G, Ma D, Zhou S, Li Z, Ni C. UHRF1-mediated ferroptosis promotes pulmonary fibrosis via epigenetic repression of GPX4 and FSP1 genes. Cell Death Dis. 2022;13:1070.
20. Warde-Farley D, Donaldson SL, Comes O, Zuberi K, Badrawi R, Chao P, et al. The GeneMANIA prediction server: biological network integration for gene prioritization and predicting gene function. Nucleic Acids Res. 2010;38:W214-220.
21. Freshour SL, Kiwala S, Cotto KC, Coffman AC, McMichael JF, Song JJ, Griffith M, Griffith OL, Wagner AH. Integration of the Drug-Gene Interaction Database (DGIdb 4.0) with open crowdsource efforts. Nucleic Acids Res. 2021; 49:D1144-D1151.
22. Aliu O, Chung KC. Assessing strength of evidence in diagnostic tests. Plast Reconstr Surg. 2012;129:989e–98e.
23. Alcala N, Leblay N, Gabriel AAG, Mangiante L, Hervas D, Giffon T, et al. Integrative and comparative genomic analyses identify clinically

relevant pulmonary carcinoid groups and unveil the supra-carcinoids. Nat Commun. 2019;10:3407.
24. Bossuyt PM, Reitsma JB, Bruns DE, Gatsonis CA, Glasziou PP, Irwig L, et al. STARD 2015: an updated list of essential items for reporting diagnostic accuracy studies. BMJ. 2015;351:h5527.
25. Liu H, Cheng Y, Yang J, Wang W, Fang S, Zhang W, Han B, Zhou Z, Yao H, Chao J, Liao H. BBC3 in macrophages promoted pulmonary fibrosis development through inducing autophagy during silicosis. Cell Death Dis. 2017;8:e2657.
26. Zhu X, Gu Y, Ma W, Gao P, Liu M, Xiao P, Wang H, Chen J, Li T. Biomarkers for Pulmonary Inflammation and Fibrosis and Lung Ventilation Function in Chinese Occupational Refractory Ceramic Fibers-Exposed Workers. Int J Environ Res Public Health. 2017; 15.
27. Yasuoka H, Garrett SM, Nguyen XX, Artlett CM, Feghali-Bostwick CA. NADPH oxidase-mediated induction of reactive oxygen species and extracellular matrix deposition by insulin-like growth factor binding protein-5. Am J Physiol Lung Cell Mol Physiol. 2019;316:L644–55.
28. Allden SJ, Ogger PP, Ghai P, McErlean P, Hewitt R, Toshner R, et al. The transferrin receptor CD71 delineates functionally distinct airway macrophage subsets during idiopathic pulmonary Fibrosis. Am J Respir Crit Care Med. 2019;200:209–19.
29. Song DG, Kim D, Jung JW, Nam SH, Kim JE, Kim HJ, Kim JH, Pan CH, Kim S, Lee JW. Glutamyl-Prolyl-tRNA synthetase regulates epithelial expression of mesenchymal markers and extracellular matrix proteins: implications for idiopathic pulmonary Fibrosis. Front Pharmacol. 2018;9:1337.
30. Yuan L, Sun Y, Zhou N, Wu W, Zheng W, Wang Y. Dihydroquercetin attenuates silica-induced pulmonary fibrosis by inhibiting ferroptosis signaling pathway. Front Pharmacol. 2022;13:845600.
31. Liang J, Huang G, Liu X, Taghavifar F, Liu N, Wang Y, et al. The ZIP8/SIRT1 axis regulates alveolar progenitor cell renewal in aging and idiopathic pulmonary fibrosis. J Clin Invest. 2022; 132.
32. Guo M, Peng T, Wu C, Pan X, Huang Z. Engineering Ferroptosis Inhibitors as Inhalable Nanomedicines for the Highly Efficient Treatment of Idiopathic Pulmonary Fibrosis. Bioengineering (Basel). 2023; 10.
33. Liu Y, Tang A, Liu M, Xu C, Cao F, Yang C. Tuberostemonine may enhance the function of the SLC7A11/glutamate antiporter to restrain the ferroptosis to alleviate pulmonary fibrosis. J Ethnopharmacol. 2024;318:116983.
34. El-Horany HE, Atef MM, Abdel Ghafar MT, Fouda MH, Nasef NA, Hegab II, et al. Empagliflozin Ameliorates Bleomycin-Induced Pulmonary Fibrosis in Rats by Modulating Sesn2/AMPK/Nrf2 Signaling and Targeting Ferroptosis and Autophagy. Int J Mol Sci. 2023; 24.
35. Cheng H, Feng D, Li X, Gao L, Tang S, Liu W, Wu X, Yue S, Li C, Luo Z. Iron deposition-induced ferroptosis in alveolar type II cells promotes the development of pulmonary fibrosis. Biochim Biophys Acta Mol Basis Dis. 2021;1867:166204.
36. He J, Li X, Yu M. Bioinformatics analysis identifies potential Ferroptosis key genes in the pathogenesis of pulmonary Fibrosis. Front Genet. 2021;12:788417.
37. He Y, Shang Y, Li Y, Wang M, Yu D, Yang Y, Ning S, Chen H. An 8-ferroptosis-related genes signature from Bronchoalveolar Lavage Fluid for prognosis in patients with idiopathic pulmonary fibrosis. BMC Pulm Med. 2022;22:15.
38. Li M, Wang K, Zhang Y, Fan M, Li A, Zhou J, et al. Ferroptosis-related genes in bronchoalveolar lavage fluid serves as prognostic biomarkers for idiopathic pulmonary fibrosis. Front Med (Lausanne). 2021;8:693959.
39. Hu Y, Huang Y, Zong L, Lin J, Liu X, Ning S. Emerging roles of ferroptosis in pulmonary fibrosis: current perspectives, opportunities and challenges. Cell Death Discov. 2024;10:301.
40. Venkatadri R, Iyer AK, Ramesh V, Wright C, Castro CA, Yakisich JS, Azad N. MnTBAP Inhibits Bleomycin-Induced Pulmonary Fibrosis by Regulating VEGF and Wnt Signaling. J Cell Physiol. 2017;232:506–16.
41. Oury TD, Thakker K, Menache M, Chang LY, Crapo JD, Day BJ. Attenuation of bleomycin-induced pulmonary fibrosis by a catalytic antioxidant metalloporphyrin. Am J Respir Cell Mol Biol. 2001;25:164–9.
42. Yao C, Guan X, Carraro G, Parimon T, Liu X, Huang G, et al. Senescence of Alveolar Type 2 cells drives progressive pulmonary fibrosis. Am J Respir Crit Care Med. 2021;203:707–17.
43. Xu Y, Mizuno T, Sridharan A, Du Y, Guo M, Tang J, et al. Single-cell RNA sequencing identifies diverse roles of epithelial cells in idiopathic pulmonary fibrosis. JCI Insight. 2016;1:e90558.
44. Minagawa S, Yoshida M, Araya J, Hara H, Imai H, Kuwano K. Regulated Necrosis in Pulmonary Disease. A Focus on Necroptosis and Ferroptosis. Am J Respir Cell Mol Biol. 2020; 62:554–562.
45. Takezaki A, Tsukumo SI, Setoguchi Y, Ledford JG, Goto H, Hosomichi K, Uehara H, Nishioka Y, Yasutomo K. A homozygous SFTPA1 mutation drives necroptosis of type II alveolar epithelial cells in patients with idiopathic pulmonary fibrosis. J Exp Med. 2019;216:2724–35.
46. Lee JM, Yoshida M, Kim MS, Lee JH, Baek AR, Jang AS, et al. Involvement of alveolar epithelial cell necroptosis in idiopathic pulmonary fibrosis pathogenesis. Am J Respir Cell Mol Biol. 2018;59:215–24.
47. Robb WB, Condron C, Moriarty M, Walsh TN, Bouchier-Hayes DJ. Taurine attenuates radiation-induced lung fibrosis in C57/Bl6 fibrosis prone mice. Ir J Med Sci. 2010;179:99–105.
48. Song L, Wang D, Cui X, Hu W. The protective action of taurine and L-arginine in radiation pulmonary fibrosis. J Environ Pathol Toxicol Oncol. 1998;17:151–7.
49. Giri SN, Wang Q. Taurine and niacin offer a novel therapeutic modality in prevention of chemically-induced pulmonary fibrosis in hamsters. Adv Exp Med Biol. 1992;315:329–40.
50. Wang QJ, Giri SN, Hyde DM, Li C. Amelioration of bleomycin-induced pulmonary fibrosis in hamsters by combined treatment with taurine and niacin. Biochem Pharmacol. 1991;42:1115–22.
51. Lin JH, Liu CC, Liu CY, Hsu TW, Yeh YC, How CK, Hsu HS, Hung SC. Selenite selectively kills lung fibroblasts to treat bleomycin-induced pulmonary fibrosis. Redox Biol. 2024;72:103148.
52. Podolanczuk AJ, Thomson CC, Remy-Jardin M, Richeldi L, Martinez FJ, Kolb M, Raghu G. Idiopathic pulmonary fibrosis: state of the art for 2023. Eur Respir J. 2023; 61.
53. Raghu G, Remy-Jardin M, Richeldi L, Thomson CC, Inoue Y, Johkoh T, et al. Idiopathic Pulmonary Fibrosis (an Update) and progressive pulmonary fibrosis in adults: An Official ATS/ERS/JRS/ALAT clinical practice guideline. Am J Respir Crit Care Med. 2022;205:e18–47.
54. Pavan B, Dalpiaz A, Marani L, Beggiato S, Ferraro L, Canistro D, et al. Geraniol pharmacokinetics, bioavailability and its multiple effects on the liver antioxidant and xenobiotic-metabolizing enzymes. Front Pharmacol. 2018;9:18.
55. Tavares LA, Rezende AA, Santos JL, Estevam CS, Silva AMO, Schneider JK, et al. Cymbopogon winterianus Essential Oil Attenuates Bleomycin-Induced Pulmonary Fibrosis in a Murine Model. Pharmaceutics. 2021; 13.
56. Wu KK. Control of tissue fibrosis by 5-methoxytryptophan, an innate anti-inflammatory metabolite. Front Pharmacol. 2021;12:759199.
57. Solopov P, Colunga Biancatelli RML, Dimitropoulou C, Catravas JD. Dietary Phytoestrogens Ameliorate Hydrochloric Acid-Induced Chronic Lung Injury and Pulmonary Fibrosis in Mice. Nutrients. 2021; 13.
58. de Baat EC, van Dalen EC, Mulder RL, Hudson MM, Ehrhardt MJ, Engels FK, et al. Primary cardioprotection with dexrazoxane in patients with childhood cancer who are expected to receive anthracyclines: recommendations from the international late effects of childhood cancer guideline harmonization group. Lancet Child Adolesc Health. 2022;6:885–94.
59. de Baat EC, Mulder RL, Armenian S, Feijen EA, Grotenhuis H, Hudson MM, Mavinkurve-Groothuis AM, Kremer LC, van Dalen EC. Dexrazoxane for preventing or reducing cardiotoxicity in adults and children with cancer receiving anthracyclines. Cochrane Database Syst Rev. 2022; 9:CD014638.
60. Von Hoff DD. Phase I trials of dexrazoxane and other potential applications for the agent. Semin Oncol. 1998;25:31–6.
61. Burgy O, Bellaye PS, Causse S, Beltramo G, Wettstein G, Boutanquoi PM, Goirand F, Garrido C, Bonniaud P. Pleural inhibition of the caspase-1/IL-1beta pathway diminishes profibrotic lung toxicity of bleomycin. Respir Res. 2016;17:162.
62. Sueblinvong V, Kerchberger VE, Saghafi R, Mills ST, Fan X, Guidot DM. Chronic alcohol ingestion primes the lung for bleomycin-induced fibrosis in mice. Alcohol Clin Exp Res. 2014;38:336–43.
63. Nagler A, Firman N, Feferman R, Cotev S, Pines M, Shoshan S. Reduction in pulmonary fibrosis in vivo by halofuginone. Am J Respir Crit Care Med. 1996;154:1082–6.
64. Baek AR, Hong J, Song KS, Jang AS, Kim DJ, Chin SS, Park SW. Spermidine attenuates bleomycin-induced lung fibrosis by inducing autophagy and

inhibiting endoplasmic reticulum stress (ERS)-induced cell death in mice. Exp Mol Med. 2020;52:2034–45.
65. Chen J, Chen S, Luo H, Wu W, Wang S. The application of arsenic trioxide in cancer: An umbrella review of meta-analyses based on randomized controlled trials. J Ethnopharmacol. 2023;316:116734.
66. Hollow SE, Johnstone TC. Realgar and arsenene nanomaterials as arsenic-based anticancer agents. Curr Opin Chem Biol. 2023;72:102229.
67. Joannes A, Morzadec C, Duclos M, Gutierrez FL, Chiforeanu DC, Le Naoures C, De Latour B, Rouze S, Wollin L, Jouneau S, Vernhet L. Arsenic trioxide inhibits the functions of lung fibroblasts derived from patients with idiopathic pulmonary fibrosis. Toxicol Appl Pharmacol. 2022;441:115972.
68. Luo F, Zhuang Y, Sides MD, Sanchez CG, Shan B, White ES, Lasky JA. Arsenic trioxide inhibits transforming growth factor-beta1-induced fibroblast to myofibroblast differentiation in vitro and bleomycin induced lung fibrosis in vivo. Respir Res. 2014;15:51.
69. Clynick B, Corte TJ, Jo HE, Stewart I, Glaspole IN, Grainge C, et al. Biomarker signatures for progressive idiopathic pulmonary fibrosis. Eur Respir J. 2022; 59.
70. Khan FA, Stewart I, Saini G, Robinson KA, Jenkins RG. A systematic review of blood biomarkers with individual participant data meta-analysis of matrix metalloproteinase-7 in idiopathic pulmonary fibrosis. Eur Respir J. 2022; 59.
71. Neighbors M, Cabanski CR, Ramalingam TR, Sheng XR, Tew GW, Gu C, et al. Prognostic and predictive biomarkers for patients with idiopathic pulmonary fibrosis treated with pirfenidone: post-hoc assessment of the CAPACITY and ASCEND trials. Lancet Respir Med. 2018;6:615–26.
72. Maher TM, Oballa E, Simpson JK, Porte J, Habgood A, Fahy WA, et al. An epithelial biomarker signature for idiopathic pulmonary fibrosis: an analysis from the multicentre PROFILE cohort study. Lancet Respir Med. 2017;5:946–55.

Publisher's Note